Numerical simulation of the drying of inkjet-printed droplets

D.P. Siregar [a,*], J.G.M. Kuerten [a,b,1], C.W.M. van der Geld [a]

[a] Department of Mechanical Engineering, Eindhoven University of Technology, P.O. Box 513, NL-5600 MB Eindhoven, Netherlands
[b] Faculty EEMCS, University of Twente, P.O. Box 217, NL-7500 AE Enschede, Netherlands

ARTICLE INFO

ABSTRACT

In this paper we study the behavior of an inkjet-printed droplet of a solute dissolved in a solvent on a solid horizontal surface by numerical simulation. An extended model for drying of a droplet and the final distribution of the solute on an impermeable substrate is proposed. The model extends the work by Deegan, Fischer and Kuerten by taking into account convection, diffusion and adsorption of the solute in order to describe more accurately the surface coverage on the substrate. A spherically shaped droplet is considered such that the model can be formulated as an axially symmetric problem. The droplet dynamics is driven by the combined action of surface tension and evaporation. The fluid flow in the droplet is modeled by the Navier–Stokes equation and the continuity equation, where the lubrication approximation is applied. The rate of evaporation is determined by the distribution of vapor pressure in the air surrounding the droplet. Numerical results are compared with experimental results for droplets of various sizes.

© 2012 Elsevier Inc. All rights reserved.

1. Introduction

For many industrial applications, inkjet printing is an important field of research. Examples of application areas are printing of ink on paper and printing DNA or protein molecules solved in a buffer fluid on microarray slides. The formulation of biomolecule solutions that give well-controlled 3D highly functional bio-layers after drying is regarded as one of the main challenges in the worldwide microarray community [1].

Microarray manufacturing starts by spotting the protein samples onto a flat horizontal surface using an inkjet printer. After the droplet collides with the surface, its kinetic energy will cause spreading and shrinking until it reaches an equilibrium shape [1–3]. The time scale from the impact to the equilibrium shape is small compared to the typical time of evaporation, which, depending on humidity and temperature, takes several seconds. Hence, the impact and the evaporation of the droplet can be separated into two independent processes.

During the evaporation phase, the dynamics of the fluid drives the protein molecules and a thin layer of deposit on the surface is formed that is partly bound to the substrate after total evaporation of the solvent. The way in which the biomolecules bind to the surface determines the functionality of the microarray [4].

Therefore, the evaporation process plays an important role in the quality of the microarray [5].

The mass transfer resulting from evaporation causes a change in the shape of the droplet. The evaporation of a sessile droplet can take place in two different ways: either the contact line moves while the contact angle remains constant, or the contact line is pinned while the contact angle decreases [6–8]. A mixed situation with a stick–slip motion of receding contact angle is also reported in literature [9]. This especially can occur during the final stages of the evaporation process. Which of the two ways of evaporation takes place depends on many parameters, for instance the hydrophobicity of the substrate, the rate of evaporation and the surface roughness.

The first model for dewetting, proposed by Young, describes the contact angle in terms of the interface tensions between air, liquid and the solid substrate. Since then, numerous studies have been conducted in order to relate the contact line behavior to the properties of the substrate. In their paper, Shin et al. [10] concluded that in the evaporation of a sessile droplet on a hydrophobic surface, in which the initial contact angle is considerable, the contact line has a higher tendency to recede. In contrast, Golovko et al. [11] determined from experiments that for a droplet with a smaller contact angle, the contact line tends to be pinned during the evaporation process. This result is supported by experimental research by Bourges-Monnier and Shanahan [12], who observed that for a contact angle smaller than 90°, the contact line is anchored during the evaporation.

One of the earliest contributions to the understanding of the dynamics of the solvent and solute was made by Deegan et al.

* Corresponding author.
E-mail addresses: d.p.siregar@tue.nl (D.P. Siregar), j.g.m.kuerten@tue.nl (J.G.M. Kuerten), c.w.m.v.d.geld@tue.nl (C.W.M. van der Geld).
[1] Principal corresponding author.

[13–15]. They assumed that the surface is so inhomogeneous that the contact line remains pinned during evaporation of the droplet. A pinned contact line is only possible if the evaporation in the area close to the contact line is compensated by convection from the center of the droplet to the edge. This process leads to the well-known coffee stain effect. An extension to this model was made by Fischer [16], who did not assume the shape of the droplet to be spherical during the evaporation process. Instead, he proposed a dynamic shape depending on the evaporation rate along the surface area. Van Dam and Kuerten [17] proposed an extension for the calculation of the curvature of the droplet shape in order to account for a droplet with a larger contact angle and considered a concentration-dependent viscosity of the liquid inside the droplet.

The singularity at the contact line is the main obstacle to model the dewetting process. The no-slip boundary condition at the liquid–substrate interface contradicts the fact that the contact line recedes with a certain velocity. This is known as the Huh and Scriven paradox [18]. One way to circumvent this singularity is by introducing slip along a small distance from the contact line which is quantified by the slip length [19–21]. Another way to solve this paradox is to use the concept of a submicroscopic precursor film [22,23]. In this approach, a thin film is assumed to cover the dry area outside the wetting area. Hence, the contact line is defined on the surface of the precursor film where fluid velocity (also called slip) is possible. In order to ensure equilibrium at the contact line, Schwartz and Eley [24] propose a model for disjoining pressure based on the Frumkin–Deryugin model, which describes the interaction between molecules.

Protein adsorption is a complex, dynamic process which involves noncovalent interactions, including hydrophobic interactions, electrostatic forces, hydrogen bonding, and van der Waals forces [25]. This process is mainly affected by the properties of the surface, the nature of the protein and the solution condition [26]. One of the earliest kinetic models is derived from the classical Langmuir equation for gas adsorption [27]. This model describes the adsorption process in the equilibrium state, by assuming that the adsorption is a purely reversible process. In later work by Lundström and McQueen [28], Beisinger and Leonard [29] and Soderquist and Walton [30], the classical steady-state Langmuir model is extended to a time-dependent model by including more complex physical phenomena such as resorption and reversible adsorption. However, validation of these models only gives a qualitative agreement with experimental results [31]. Kurat et al. developed an adsorption model for bovine serum albumin at silica–titania surfaces [32,33]. They showed that their theoretical model is in good agreement with their experimental results.

In this paper, we present a numerical method for the fluid dynamics and the motion and final deposition of solute molecules during the evaporation of an inkjet-printed droplet on a solid substrate. The method is based on models for flow of the liquid, convection and diffusion of the solute and binding of the solute molecules to the substrate. We will compare results of the model with experimental results for droplets of various sizes and perform a sensitivity study by varying the most important physical parameters in the models.

2. Mathematical models

The mathematical model covers the dynamics of the solvent due to evaporation, the concentration of the solute and the binding of the solute molecules to the surface. We consider two separate cases for the contact line dynamics: a pinned and an unpinned contact line. As we consider dilute solutions we neglect the influence of concentration on viscosity. Fig. 1 depicts an axially symmetric droplet (a spherical cap) on a horizontal substrate with H and R the initial height and radius respectively, and θ_c the contact angle.
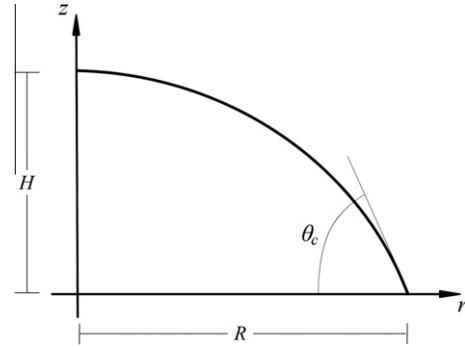

Fig. 1. Sketch of a spherical droplet on an impermeable substrate.

2.1. Lubrication equation

A complete model for the flow inside the droplet is provided by the three-dimensional Navier–Stokes equation and the continuity equation for an incompressible fluid. However, a study of the order of the magnitude of the terms in these equations reveals that the model can be simplified by the lubrication approximation. Moreover, only situations with cylindrical symmetry, in which the quantities do not depend on the azimuthal coordinate and the azimuthal velocity equals zero, will be considered. The most important assumptions in this simplified model are that the height of the droplet is much smaller than its radius and that the height of the drop is well below the capillary length. The capillary length is defined as $l_\sigma = (\sigma/\rho g)^{1/2}$, where σ and ρ denote surface tension and mass density of the liquid and g the acceleration of gravity. This second assumption implies that the influence of gravity is negligible [23,34]. For a thin droplet with a small contact angle, the first assumption can be written as $\epsilon = H/R \ll 1$. These assumptions lead to a simplified form of the Navier–Stokes equation [35,16,17,36], where the radial velocity component u can explicitly be determined from the pressure p at the liquid–air interface.

The shape of the droplet $h(r,t)$ is determined by conservation of mass, which incorporates changes in shape due to the flow inside the droplet and due to evaporation

$$\frac{\partial h}{\partial t} = \frac{1}{3\mu} \frac{1}{r} \frac{\partial}{\partial r}\left(rh^3 \frac{\partial p}{\partial r}\right) - J(r), \tag{1}$$

where μ is the dynamic viscosity and $J(r)$ indicates the evaporation velocity, which may depend on the radial coordinate. This equation holds for both pinned and unpinned contact lines. The pressure within the droplet is dominated by the effect of surface tension. At the liquid–air interface, the pressure difference between the droplet and the air is given by the Laplace pressure:

$$p = p_L = -\sigma \frac{1}{r} \frac{\partial}{\partial r}\left(\frac{r \frac{\partial h}{\partial r}}{\sqrt{1 + \left(\frac{\partial h}{\partial r}\right)^2}}\right). \tag{2}$$

The term in the denominator takes into account the exact radius of curvature of an axially symmetric drop and makes it possible to extend the range of validity of the approach to larger contact angles than possible when the lubrication approximation is made. Consequently, the equilibrium shape of the droplet is a spherical cap instead of a parabola, which is the equilibrium shape in the lubrication approximation.

For an unpinned contact line, the mass loss due to evaporation causes the contact line to move to the center of the droplet keeping a constant contact angle. However, at the contact line a singularity exists due to no-slip boundary condition at the liquid–substrate interface which is known as Huh and Scriven's paradox [18]. In

order to circumvent this singularity and use the same evolution equation for the droplet height, a thin film is assumed to cover the dry part of the substrate and the contact line dynamics are defined at the surface of the thin film. In order to ensure the equilibrium of the contact angle, the dewetting process is modeled by adopting a disjoining pressure proposed by Schwartz and Eley [24]. The pressure in the droplet is given by

$$p = -P_L - \Pi, \tag{3}$$

where P_L is the Laplace pressure defined in Eq. (2). The disjoining pressure Π is defined in such a way that it is zero outside the wetting area:

$$\Pi(h) = B\left(\left(\frac{h^*}{h}\right)^n - \left(\frac{h^*}{h}\right)^m\right), \tag{4}$$

where B, n, and m are positive constants and h^* is the thickness of the precursor film. In order to satisfy the balance of capillary and disjoining pressure forces parallel to the substrate, the parameter values are given by $n = 3$ and $m = 2$, where the thickness of the precursor film is given by h^*. The value of B is determined by

$$B = \frac{1}{h^*} \frac{(n-1)(m-1)}{2 (n-m)} \sigma \theta_e^2, \tag{5}$$

where θ_e is the defined equilibrium contact angle. A more detailed discussion on this topic can be found in Schwartz [24,37] and Alleborn et al. [38,39]. In this paper we use a value of $h^* = h/100$, which corresponds to the typical height of a precursor film found in literature [38,39].

2.2. Concentration model

The change in solute concentration during the evaporation process is caused by three factors: the loss of solvent, the dynamics of the fluid and the adsorption of solute molecules to the substrate. The loss of solvent causes an increase of the solute concentration and leads to transport of solute by convection and diffusion. Adsorption leads to a local decrease of solute concentration. Hence, the concentration of the solute is governed by a two dimensional convection–diffusion equation

$$\frac{\partial C}{\partial t} = -\frac{1}{r} \frac{\partial}{\partial r}(r\, C\, u) - \frac{\partial}{\partial z}(C\, w) + D\frac{1}{r}\frac{\partial}{\partial r}\left(r\frac{\partial C}{\partial r}\right) + D\frac{\partial^2 C}{\partial z^2}$$
$$- F\delta(z), \tag{6}$$

where C is the solute concentration, u and w are radial and axial velocity components, respectively, and $\delta(z)$ is the delta function. The function F, which will be defined later, describes the mass loss of the solute due to the binding between molecules and surface, which is defined only on the surface $z = 0$.

The convection–diffusion equation for the concentration not only involves the radial velocity component u, but also the vertical velocity component w. The radial velocity component can easily be solved from the governing equations in the lubrication approximation and is related to the pressure by

$$u = \frac{1}{\mu}\left(\frac{1}{2}z^2 - hz\right)\frac{\partial p}{\partial r}. \tag{7}$$

The vertical velocity component can be found from u by solving the continuity equation with a no-slip boundary condition on the surface.

2.3. Evaporation model

In microarray manufacturing, the evaporation process takes place under isothermal conditions. Evaporation of the droplet is induced by a normal gradient of vapor pressure at the droplet–liquid interface. The vapor pressure gradient depends on the relative humidity in the ambient air and on the temperature-dependent saturation pressure. In order to incorporate evaporation into Eq. (1) for the droplet height, an expression for the evaporation velocity J as a function of the radial coordinate is required.

The evaporation velocity J depends on the rate-limiting step, which can be either the transfer rate across the liquid–vapor interface or the diffusion of the saturated vapor layer directly above the droplet. For droplets of micrometer size, the typical time for diffusion of vapor is of the order of 10^{-6} s, while the typical time for the transfer rate across the interface is of the order to 10^{-10} s [40]. Therefore, it can be concluded that the diffusion of saturated vapor is the limiting step.

Since the diffusion is the rate-limiting step, and by assuming that the evaporation rapidly attains a steady state condition, the vapor mass density n has to satisfy the Laplace equation in the air surrounding the droplet. The boundary conditions are that the vapor mass density equals the saturated vapor mass density at the interface n_s and equals the bulk vapor mass density far away from the interface n_∞. The boundary condition on the dry part of the substrate, $\partial n/\partial z = 0$ corresponds to a zero flux condition. By determining the vapor mass density, the evaporation flux given by Fick's law, $j = -\mathscr{D}\nabla n$, where $\mathscr{D}$ is the diffusion coefficient, can be calculated.

For a given droplet shape $J(r)$ can be calculated in this way. It would, however, require quite some computational effort to solve the Laplace equation for the vapor concentration in every time step of the evaporation process. Therefore, we make the approximation that the droplet shape corresponds to a spherical cap with the same actual values of droplet radius and contact angle and we applied the analytical expression for the evaporation velocity given by Popov [40].

In order to investigate the effect of changing contact angle we will compare the results with two limiting cases. In the first we use Popov's small contact angle approximation [40]:

$$J(r) = \frac{2}{\pi} \frac{\mathscr{D}(n_s - n_\infty)}{\rho\sqrt{R^2 - r^2}} \sqrt{1 + \left(\frac{\partial h}{\partial r}\right)^2}. \tag{8}$$

The other limiting case appears when the contact angle is 90° and the droplet is half a sphere. In that case the vapor concentration at the liquid–air interface is constant and the evaporation velocity does not depend on the radial coordinate and is given by that of a spherical droplet as:

$$J(r) = \frac{\mathscr{D}(n_s - n_\infty)}{\rho R}\sqrt{1 + \left(\frac{\partial h}{\partial r}\right)^2}. \tag{9}$$

2.4. Adsorption model

The adsorption of the solute determines the surface coverage and the functionality of the biomolecule. Here we make use of a model by Kurrat et al. [33] where the adsorption of protein molecules can happen in a reversible and an irreversible way. We will indicate the adsorbed mass per unit area of the two types by M_r and M_i respectively [32]. The model can be written as:

$$\frac{\partial M_r}{\partial t} = k_a C\phi - \frac{k_d M_r}{\sqrt{\phi}}, \tag{10}$$

$$\frac{\partial M_i}{\partial t} = k_s C\phi, \tag{11}$$

where k_a and k_s are rate constants for reversible and irreversible adsorption, respectively and k_d is the rate constant for desorption. These constants can be determined experimentally and depend on the type of protein, on the buffer that is used and on the properties

of the substrate. The variable ϕ defines the fraction of surface area that can be occupied by the solute particles, given by the Langmuir expression $\phi = 1 - \theta$ [41]. Here, θ is related to the total adsorbed mass per unit area $M = M_r + M_i$ by $\theta = Ma/m$ where a is the area occupied by a single molecule and m is the mass of a single molecule.

Using conservation of solute mass, the rate of solute mass loss is defined as the sum of the rates for reversible and irreversible adsorption

$$F = k_a C \phi - \frac{k_d M_r}{\sqrt{\phi}} + k_s C \phi. \tag{12}$$

3. Numerical results and analysis

The governing equations constitute a set of coupled nonlinear partial differential equations with a maximum derivative with respect to the radial coordinate of fourth order. The partial differential equations cannot be solved analytically, so that a numerical method is needed. We use the advantages of the method of lines [42] to transform the partial differential equations into a system of ordinary differential equations. The space domain is discretized using a finite volume method in order to guarantee the conservation of mass. The spatial derivatives can easily be approximated by either an upwind scheme or central differences. The time integration has to be treated separately for each equation due to different stability conditions. Accordingly, the time integration is solved with a combination of a fifth-order accurate Gear method and a first-order accurate implicit Euler method. The numerical method is programmed in Fortran and executed using parallel computing on a shared memory machine with the use of Openmp.

3.1. Validation

The validation of the lubrication approach and of the evaporation model is presented in this subsection. Numerical results are compared with experimental results for two different cases, which differ in the size of the initial droplet. The first case concerns a microliter droplet with a typical volume of 10^{-6} L and the second case is a picoliter droplet with a typical volume of 10^{-12} L. The experimental results are obtained by Hu and Larson [43] and Golovko et al. [11].

The experiment by Hu et al. was performed with a water droplet deposited on a clean glass cover slip, where the contact line remained pinned during the evaporation process. Hence, this result is compared with a simulation for a droplet without solute with a pinned contact line. The experimental result is compared with the analytical expression of the evaporation model and with the two limiting cases. The physical properties that are used in experiment and simulation are presented in Table 1.

Fig. 2 depicts the droplet height and the contact angle as functions of time. It can be seen that the best agreement is given by the simulation result with the analytical expression of the evaporation model. The limiting cases deviate from the analytical model where the limiting case for a small contact angle gives a better agreement with the experimental result. This is due to relatively small initial contact angle of the droplet. Hence this comparison confirms the evaporation model for the microliter droplet.

The experiment by Golovko et al. was performed with a water droplet on a hydrophilic surface, which causes the contact line to be pinned during the evaporation process. Therefore, this result is also compared with a simulation for a droplet without solute with a pinned contact line. For the given droplet volume and initial contact angle, the initial radius and height of the droplet are calculated by assuming that the initial shape is a spherical cap. This

Table 1
Physical data for the simulation of the microliter droplet. This data is obtained from the paper by Hu and Larson [43].

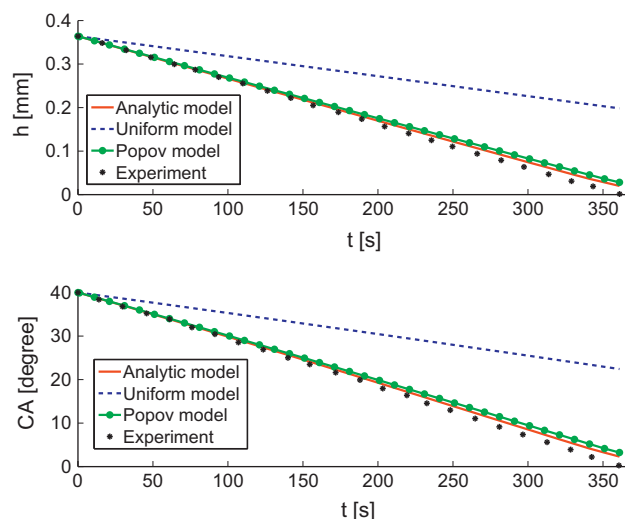| Parameter	Symbol	Value
Initial volume	V	0.597 µL
Initial contact angle	θ_e	40 deg
Dynamic viscosity	μ	0.89 mPa s
Surface tension	σ	72.994 mN m^{-1}
Mass density	ρ	997.048 kg m^{-3}
Temperature	T	298 K
Relative humidity	RH	0.4
Vapor pressure	P_{sat}	3.158 kPa

Fig. 2. Comparison between numerical and experimental results for a droplet with initial volume 0.597 µL and relative humidity $RH = 0.4$.

corresponds to the shape in which all acting forces are in equilibrium. The physical properties that are used in experiment and simulation are presented in Table 2.

Results of the simulations and the experiment are depicted in Fig. 3. In this figure the volume is plotted as the function of time. The simulation is stopped after a simulation time of 0.47 s, which equals the duration of the experiment.

The numerical model results in a similar behavior of droplet volume, in which the volume decreases linearly in time. Hence, the value of the mass loss is almost constant in time for all models with an average of approximately 7.5×10^{-5} µL/s. The experimental results show a similar behavior, but with an evaporation rate approximately twice as high. The volume decreases linearly in time with an average mass loss is equal to 15×10^{-5} µL/s and after 0.45 s the liquid is almost totally dried.

Table 2
Physical data for the simulation of the picoliter droplet. This data is obtained from the paper by Golovko et al. [11].

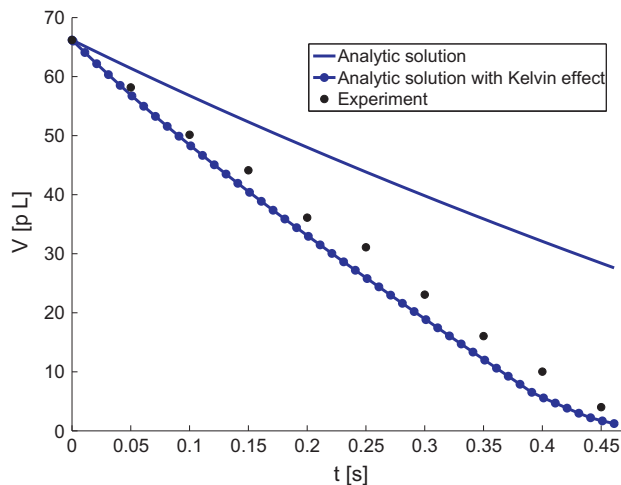| Parameter	Symbol	Value
Initial volume	V	66.2 µL
Initial contact angle	θ_e	70 deg
Dynamic viscosity	μ	0.89 mPa s
Surface tension	σ	72.994 mN m^{-1}
Water mass density	ρ	997.048 kg m^{-3}
Temperature	T	298 K
Relative humidity	RH	0.3
Vapor pressure	P_{sat}	3.158 kPa

Fig. 3. Comparison between numerical models with correction factor due to the Kelvin effect and experimental result for a droplet with initial volume 66.2 μL and relative humidity $RH = 0.3$.

One possible cause for differences between experimental and numerical results is the model assumption that the temperature of the droplet is constant during the evaporation process. Due to the evaporation and the associated latent heat the droplet will be locally cooled at the interface. In the model it is assumed that the heat conduction in the droplet and the heat transfer between the droplet and the substrate are sufficiently high to compensate this energy loss and maintain a uniform temperature. Especially for small droplets this assumption could become questionable since the ratio of interface area and volume increases. However, a lower temperature of the interface would result in a lower saturation pressure and hence a smaller value of n_s and x_0 in the expressions for the evaporation velocity $J(r)$. Hence, the temperature change would result in a lower mass loss than predicted by the present model and this mechanism cannot explain the difference between the experimental and numerical results.

It is known that the rate of evaporation of a sessile droplet reaches its maximum at the edge of the droplet. Due to this fact, other possible explanations for the discrepancies between measured and predicted evaporation rate can therefore be sought in an underestimation of the evaporation rate near the contact line. The saturation pressure near the drop surface depends on the curvature, an effect that goes by the name of the Kelvin effect [44]. This is a negligible effect unless the mean radius of curvature becomes very small, of the order of 100 nm to 1 μm in the case of a water–air interface. It was shown by Golovko et al. that a precursor film extends from the contact line to the outskirts of the substrate. Near the contact line the curvature is probably large enough to invoke the Kelvin effect. Evaporation from the precursor film might also occur, but a high velocity liquid flow into the film would be necessary to account for the necessary total evaporation rate. This phenomenon was studied in the work of Pham et al. [45], where it was shown theoretically that the suction of the liquid due to the low pressure around the contact line allows the liquid to evaporate in the precursor film. In addition, the tip of the precursor film can also invoke the Kelvin effect which furthermore increase the evaporation rate. Due to the limitations of the current model, we simulate the occurrence of the Kelvin effect near the contact line as a possible cause for a high evaporation rate in the experiments and will now proceed to show that this effect alone suffices to obtain proper model predictions.

In order to do this, the Kelvin effect is accounted for locally near the contact line with the aid of the following expression for the ratio of the actual saturation pressure at a curved interface P^* with a mean radius of curvature given by R_s to the saturation pressure occurring at a flat interface P_{sat} under otherwise similar conditions,

$$\ln\left(\frac{P^*}{P_{sat}}\right) = \frac{2\sigma V_m}{R_s R_u T}, \tag{13}$$

where $V_m = M_v/\rho_v$. In order to investigate the significance of this effect for the simulations, the radius of curvature has been decreased by a factor of ten in an interface area with a reasonable size of 1 μm. The result of the inclusion of the correction factor is included in Fig. 3. It can be seen that the evaporation rate increases approximately by a factor of two, so that the results of the numerical model is now in the same order of magnitude as the experimental result. Hence, the Kelvin effect near the contact line suffices to explain the difference between the models and experiment. In general, the inclusion of the Kelvin effect gives a better agreement with the experimental results in all three models. However, the present estimates for radii of curvature and area of importance are heuristic, although realistic, and further investigations are necessary to include this phenomenon properly in the model. Because of this, the Kelvin phenomenon is not applied in the remaining of this study.

3.2. Droplet evolution and comparison

In this subsection the results of numerical simulations for both pinned and unpinned contact line are presented and compared. The numerical results in this section are presented in dimensionless forms by scaling the droplet height with initial droplet height H, the radius of the droplet with initial droplet radius R, the solute concentration C with initial solute concentration C_0 and the adsorbed mass per unit area with $M_0 = C_0 H$.

In this example, we use the same physical data as presented in Table 1. Furthermore, for the solute particles properties we use $C_0 = 200$ μg mL^{-1}, $k_a = k_s = 1.1 \times 10^{-8}$ m s^{-1} and $k_d = 0.44 \times 10^{-4}$ s^{-1}. The adsorption coefficients correspond to the adsorption process of the bovine serum albumin (BSA) protein with HEPES (4-(2-hydroxy-ethyl)-1-piperazine-ethane-sulfonic acid) as the buffer at silica–titania surfaces.

Fig. 4 depicts the shape history of the droplet with a pinned contact line during the evaporation process at several equidistant instances in time. The figure shows a gradual decrease of the droplet height with a constant contact radius during the evaporation. The pinning induces convection from the center of the droplet to the edge in order to keep pace with the evaporation in the area close to the contact line. This convection causes a migration of solute particles and increases the solute concentration in the region close to the contact line. This process is illustrated in Fig. 5 by the layer thickness Ch, which is the integral of solute concentration over the height of the droplet, as a function of the radial coordinate. During the latest stages of the evaporation process, nearly all solute particles have been transported to the edge of the droplet. This process causes the adsorbed solute particles to accumulate in the area near the contact line, due to the linear relation between the adsorption rate and the solute concentration given by Eqs. (10) and (11). This explains the behavior of the surface coverage shown in Fig. 6.

A different evolution of droplet shape can be seen in Fig. 7. In this figure, the gradual decrease of the droplet includes the movement of the contact line toward the center of the droplet with a constant contact angle. Due to the presence of the disjoining pressure, which stems from the inter-molecular interactions, the shape of the droplet interface near the contact line clearly differs from the parabolic profile of the pinned contact line. The unpinned contact line induces a convective flow toward the center due to the
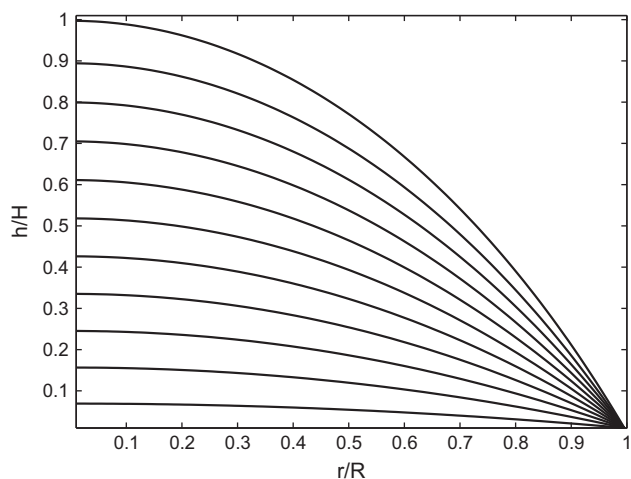
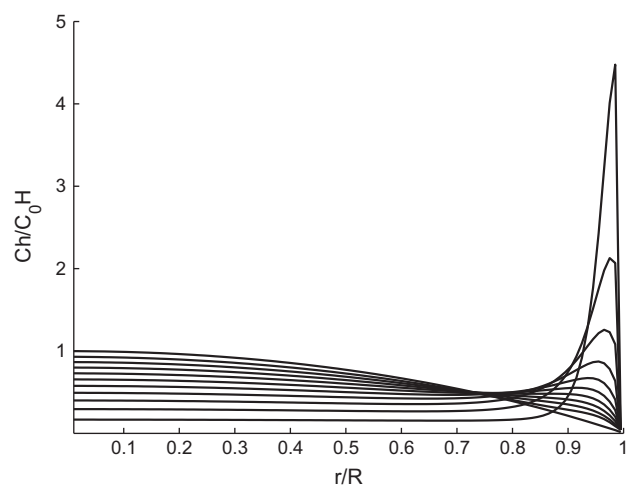**Fig. 4.** Evolution of the shape of the droplet with a pinned contact line.

Fig. 7. Evolution of the shape of the droplet with an unpinned contact line.

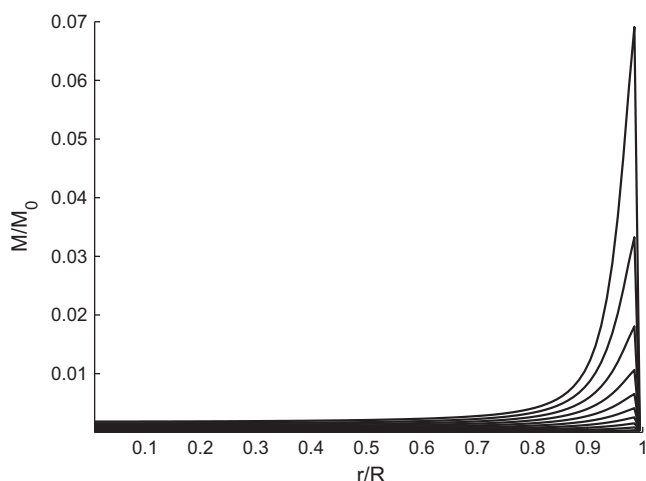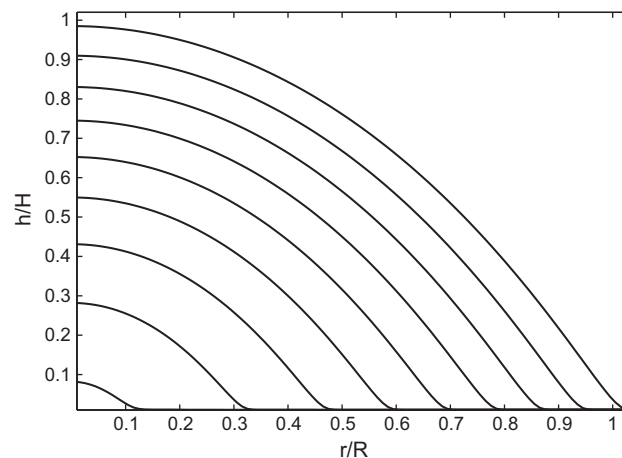influence of surface tension, which tries to maintain the droplet in a spherical cap shape.

Due to the dominance of convection over diffusion, the convective flow drives the solute particles toward the center of the droplet. As the contact line moves toward the center of the droplet, the convective flow transports the solute particles near the contact line region. Since the contact line velocity is faster than the flow near the contact line, most of the solute particles accumulate near the contact line. This increases the concentration near the dynamic contact line, which is indicated by the concentration peak in Fig. 8.

As already shown in the case of the pinned contact line, the adsorption rate is strongly influenced by the concentration of solute particles near the surface of the substrate. Therefore, the adsorption profile depicted in Fig. 9 shows a different behavior than in the pinned droplet case. In the case of an unpinned contact line, the evaporation process causes most of the adsorbed solute particles to accumulate near the center of the droplet except for a small area around $r = 0$.

Fig. 10 shows the time evolution of the droplet volume for both cases, from which the drying time can be inferred. It can be seen that the drying time of a droplet with a pinned contact line is shorter than for a droplet with an unpinned contact line. This is due to the larger droplet surface area in the pinned case, as the instantaneous mass loss increases with increasing surface area.
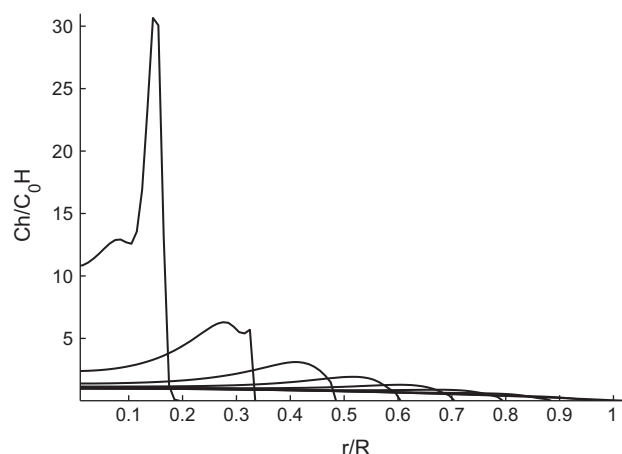

Fig. 5. Evolution of the layer thickness of the solute for the droplet with a pinned contact line.

Fig. 6. Evolution of adsorbed solute mass per unit area for the droplet with a pinned contact line.

Fig. 8. Evolution of the layer thickness of the solute for a droplet with an unpinned contact line.
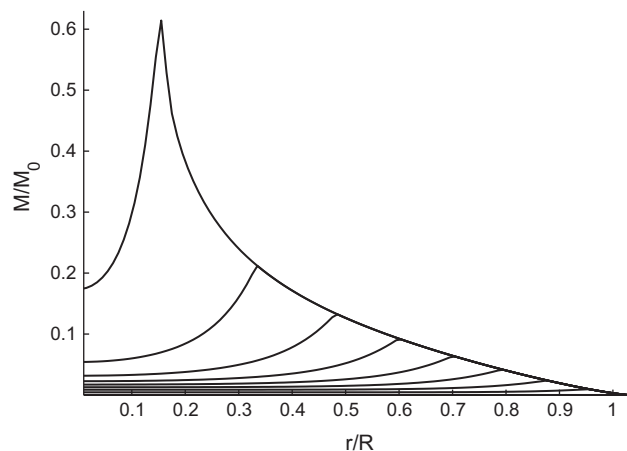
Fig. 9. Evolution of solute mass adsorption per unit area for a droplet with an unpinned contact line.
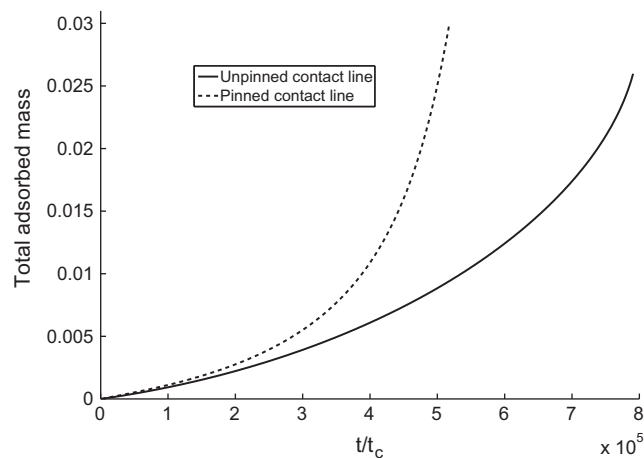

Fig. 11. Total adsorbed solute mass as a function of time for a droplet with a pinned and an unpinned contact line.
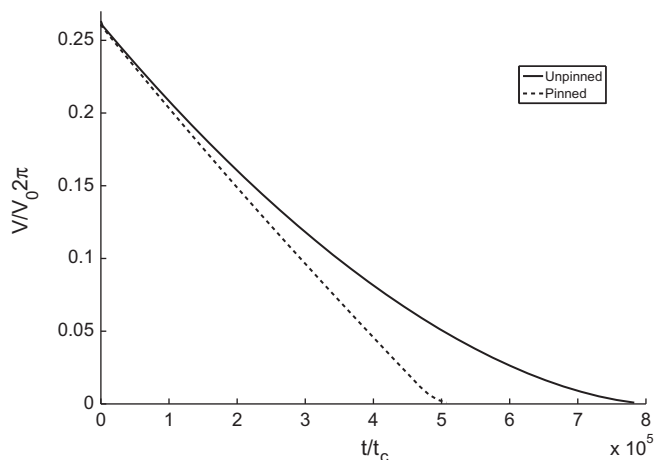

Fig. 10. Droplet volume as a function of time for the pinned and unpinned contact line.

The condition of the contact line also influences the amount of solute particles that is adsorbed by the substrate surface. Fig. 11 depicts the total adsorbed mass as a function of time. It can be seen that the total adsorbed mass for the evaporation of the droplet with a pinned contact line is higher. This is due to the contact line pinning, which provides a larger area to be occupied by the particles resulting in a higher adsorption rate. Note that at the end of the drying process, not all solute molecules need to be adsorbed by the substrate. Depending on the initial solute concentration and the speed of the drying process, a number of molecules will be lying on top of the substrate and will not contribute to the functioning of the microarray.

4. Conclusions

We have developed a numerical model for simulating the drying of inkjet printed droplets. A number of assumptions have been made in order to reduce the complexity of the governing equations and the computation time. In particular, we have used the lubrication theory in order to simplify the full Navier–Stokes equation. The validity of these assumptions has been tested by comparing the numerical results with experimental results. Although this validation was limited to certain physical properties, such as the droplet morphology, this comparison has shown a fair agreement.

This confirms the accuracy of the lubrication approach. However, the assumptions limit the applicability of the current numerical model to the evaporation and absorption of sessile droplets with contact angle less than 90°. The model can be extended into a two-dimensional model in order to cover the case of droplets with a larger contact angle. However, this approach will greatly increase the complexity of the numerical algorithm and the computation time.

The analytical evaporation model has been implemented and compared with experimental results. For a droplet with a volume of 0.597 μL, the evaporation model gives a good agreement with the experimental results. However, the current model is not able to simulate the evaporation process for much smaller droplets. This is due to certain physical circumstances that cannot yet be included in the model. Some relevant suggestions have been formulated that can be used as a starting point for more detailed modeling approaches. In particular inclusion of the Kelvin effect related to the presence of a precursor film bounding the droplet is a promising extension of the current model to obtain better agreement for very small droplets.

Our study also showed the influence of the contact line condition on the drying process. It can be seen that this condition strongly influences the morphology of the solute deposit and the adsorption profile.

References

[1] J.F. Dijksman, A. Pierik, Biomicrofluidics 2 (044101) (2008).
[2] J.P. Dear, J. Field, J. Appl. Phys. 63 (1988) 1015–1021.
[3] J.E. Field, M.B. Lesser, J.P. Dear, Proc. Roy. Soc. Lond. Ser. A, Math. Phys. Sci. 401 (1821) (1985) 225–249.
[4] M. Dufva, Biomol. Eng. 22 (5–6) (2005) 173–184.
[5] B. Rieger, L. van den Doel, L. van Vliet, Phys. Rev. E 68 (036312) (2003).
[6] E. Bonacurso, H.J. Butt, J. Phys. Chem. B 109 (1) (2005) 253–263.
[7] D. Orejon, K. Sefiane, M. Shanahan, Langmuir (2011).
[8] R. Picknett, R. Bexon, J. Colloid Interf. Sci. 61 (2) (1977) 336–350.
[9] K.S. Birdi, D.T. Vu, A. Winter, J. Phys. Chem. 93 (1989) 3701–3703.
[10] D. Shin, S. Lee, J. Jung, J. Yoo, Microelectron. Eng. 86 (2009) 1350–1353.
[11] D.S. Golovko, H.J. Butt, E. Bonaccurso, Langmuir 25 (2009) 75–78.
[12] C. Bourges-Monnier, M.E.R. Shanahan, Langmuir 11 (1995) 2820–2829.
[13] R.D. Deegan, Phys. Rev. E 61 (1) (2000) 475–485.

[14] R.D. Deegan, O. Bakajin, T.F. Dupont, G. Huber, S.R. Nagel, T.A. Witten, Nature 389 (1997) 827–829.
[15] R.D. Deegan, O. Bakajin, T.F. Dupont, G. Huber, S.R. Nagel, T.A. Witten, Phys. Rev. E 62 (1) (2000) 756–765.
[16] B.J. Fischer, Langmuir 18 (2002) 60–67.
[17] D.B. van Dam, J.G.M. Kuerten, Langmuir 24 (2008) 582–589.
[18] C. Huh, L.E. Scriven, J. Colloid Interf. Sci. 35 (1) (1971) 85–101.
[19] V.E.B. Dusan, Annu. Rev. Fluid Mech. 11 (371–400) (1979).
[20] C. Huh, S.G. Mason, J. Colloid Interf. Sci. 60 (1) (1975) 11–38.
[21] J. Lowndes, J. Fluid Mech. 101 (1980) 631–646.
[22] P.G. de Gennes, Rev. Mod. Phys. 57 (3) (1985) 827–863.
[23] P.G. de Gennes, F. Brochard-Wyart, D. Quere, Capillarity and Wetting Phenomena, Springer, 2004.
[24] L. Schwartz, R. Eley, J. Colloid Interf. Sci. 202 (1998) 173–188.
[25] J.D. Andrade, V. Hlady, Adv. Polym. Sci. 79 (1986) 1–63.
[26] J.D. Andrade, Surface and Interfacial Aspects of Biomedical Polymers, Surface Chemistry and Physics, vol. 1, Kluwer Academic, 1985.
[27] A.W. Adamson, A.P. Gast, Physical Chemistry of Surfaces, Wiley-Interscience, New York, 1997.
[28] I. Lundström, D. McQueen, J. Theor. Biol. 45 (2) (1974) 405–409.
[29] R.L. Beissinger, E.F. Leonard, J. Colloid Interf. Sci. 85 (2) (1982) 521–533.
[30] M. Soderquist, A. Walton, J. Colloid Interf. Sci. 75 (2) (1980) 386–397.
[31] I. Lundström, H. Elwing, J. Colloid Interf. Sci. 136 (1) (1990) 68–84.
[32] R. Kurrat, J.E. Prenosil, J.J. Ramsden, J. Chem. Soc. Faraday Trans. 90 (4) (1994) 587–590.
[33] R. Kurrat, J.E. Prenosil, J.J. Ramsden, J. Colloid Interf. Sci. 185 (CS964528) (1997) 1–8.
[34] J. Snoeijer, E. Rio, N.L. Grand, L. Limat, Phys. Fluids 17 (072101) (2005).
[35] S. Howison, Practical Applied Mathematics: Modelling, Analysis, Approximation, The Edinburgh Building, vol. 1, Cambridge University Press, Cambridge, UK, 2005.
[36] J.G.M. Kuerten, D.P. Siregar, Inkjet-based Micromanufacturing, Wiley-VCH, 2012.
[37] L.H. Schwartz, Theoretical and numerical modeling of coating flow on simple and complex substrates including rheology, drying and Marangoni effects, in: F. Durst, H. Raszillier (Eds.), Advances in Coating and Drying of Thin Films, Shaker Verlag, 1999, pp. 105–128.
[38] N. Alleborn, H. Raszillier, Spreading and sorption of droplets on layered porous substrates, J. Colloid Interf. Sci. 280 (2004) 449–464.
[39] N. Alleborn, H. Raszillier, Chem. Eng. Sci. 59 (2004) 2071–2088.
[40] Y. Popov, Phys. Rev. 171 (036313) (2005).
[41] R.G. Mortimer, Physical Chemistry, second ed., Academic Press, 2000.
[42] C. Großmann, H.G. Roos, Numerik partieller Differentialgleichungen, Teubner Verlag, 2003.
[43] H. Hu, R.G. Larson, J. Phys. Chem. B 106 (2002) 1334–1344.
[44] A. Thomson, Philos. Mag. 4 (1871) 448–452.
[45] C. Pham, G. Berteloot, F. Lequeux, L. Limat, EPL 92 (54005) (2010).